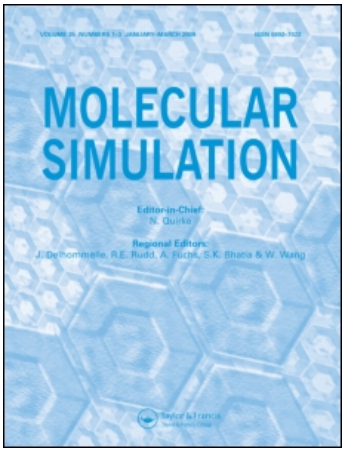

Molecular Simulation
Publication details, including instructions for authors and subscription information:
http://www.informaworld.com/smpp/title~content=t713644482

Simulation of Colloid-Polymer Systems using Dissipative Particle Dynamics

Jonathan B. Gibson[a]; Kai Zhang[b]; Ke Chen[a]; Simon Chynoweth[c]; Charles W. Manke[b]
[a] Department of Mathematical Sciences, University of Liverpool, Liverpool, U.K. [b] Wayne State University, Detroit, Michigan [c] Shell Global Solutions, Chester, U.K.

To cite this Article Gibson, Jonathan B. , Zhang, Kai , Chen, Ke , Chynoweth, Simon and Manke, Charles W.(1999) 'Simulation of Colloid-Polymer Systems using Dissipative Particle Dynamics', Molecular Simulation, 23: 1, 1 — 41
To link to this Article: DOI: 10.1080/08927029908022109
URL: http://dx.doi.org/10.1080/08927029908022109

Molecular Simulation, 1999, Vol. 23, pp. 1–41
Reprints available directly from the publisher
Photocopying permitted by license only

SIMULATION OF COLLOID-POLYMER SYSTEMS USING DISSIPATIVE PARTICLE DYNAMICS

JONATHAN B. GIBSON[a,*], KAI ZHANG[b], KE CHEN[a], SIMON CHYNOWETH[c] and CHARLES W. MANKE[b]

[a] *Department of Mathematical Sciences, University of Liverpool, Liverpool, U.K. L69 3BX;*
[b] *Wayne State University, Detroit, Michigan 48202;*
[c] *Shell Global Solutions, Thornton, P.O. Box 1, Chester, U.K. CH1 3SH*

(Received January 1999; accepted March 1999)

Dissipative particle dynamics (DPD), a tool for simulating the hydrodynamic behaviour of complex fluids, was recently successfully applied to a new application – modelling the adsorption of colloidal particles onto a polymer coated surface. Here, we both improve our model for the simulation of colloid-polymer systems and broaden its application. A virtual wall has been added to the model for colloidal particle adsorption, allowing the density of particles in the wall to be the same as in the solvent. This eliminates the depletion layer and thus also enables the potential between a colloidal particle and the wall to be calculated. We use two alternative wall models, the *solid wall* and the *porous wall*, to study the process of polymer adsorption. Simulations are also conducted in order to understand, and hence reduce, the problem of polymer crossing and to study the viscosity of various colloid-polymer systems.

Keywords: Dissipative particle dynamics; complex fluids; adsorption; polymer crossing; viscosity

1. INTRODUCTION

Many practical applications in colloid science concern the interaction of particles, polymers and surfaces. An earlier paper [1] studied, for the first time, the application of the technique of dissipative particle dynamics to this problem. Due to the absence of suitable alternative techniques for simulating the hydrodynamic behaviour of colloid-polymer-solvent systems, this

*Corresponding author.

earlier paper was concerned with assessing the potential of DPD for such simulations and at the same time, establishing a framework for the simulation of the wider, and more generic, problem. Specifically, the introductory study concerned the adsorption of colloidal particles onto a polymer coated surface. This can be applied to problems such as the control of surface fouling in chemical reactors and the design of detergents to control redeposition of dirt on fabric after washing.

The motivation behind this work is the problem of controlling the effects of soot in diesel engine lubricating oil. The oil becomes contaminated by soot particles of 10 to 50 nm in size created by incomplete fuel combustion. Agglomeration of this soot adversely affects the viscosity of the oil and so dispersants are added to the oil in an attempt to control this [2]. Ultimately, it is hoped that a model can be developed using the dissipative particle dynamics [3, 4] simulation technique which will allow us to better understand and hence optimise the conditions that affect such a system. Results from the earlier work, simulating particle adsorption onto a polymer coated surface, show good agreement with theoretical predictions. This report will first detail refinements made to the generic model and then describe how it has been developed to study different aspects of a colloid-polymer system.

Dissipative particle dynamics was originated in 1992 by Hoogerbrugge and Koelman [3, 5] as a flexible and computationally efficient tool for performing fluid dynamics simulations of complex fluids. It was found to produce a flow of momentum through space that is effectively "identical" to that resulting from the classical equations of motion. An important advance was made to the model in 1995 when the fluctuation-dissipation theorem of Español and Warren [4] was formulated. DPD has been applied to a number of applications, including the study of polymer solutions [6, 7, 8], binary fluid systems [9, 10] and the rheological properties of dense colloidal suspensions [11, 12]. In each case the simulations have been very successful in reproducing the expected behaviour.

The next section of this report provides an overview of the DPD technique. §3 describes the simulation results obtained by using an improved model for the adsorption of colloidal particles onto a polymer coated surface. §4 details the simulation work carried out to investigate the process of polymer adsorption onto a surface. The sections which follow describe an investigation conducted in order to reduce the problem of polymer crossing and an investigation into the viscosity of various colloid-polymer systems. Conclusions are drawn in the final section of the report.

2. THE DPD SIMULATION METHOD

In DPD, the fluid is considered to be made up of N discrete, interacting, point *particles*, moving in a continuum domain of volume V. Since DPD is a mesoscopic simulation technique, these *particles* do not represent actual molecules but groups of molecules, or alternatively they can be thought of as fluid packets. Periodic boundary conditions are applied to produce image boxes that mimic the behaviour of an infinitely large system. Similar to molecular dynamics (MD), a configuration of the fluid is fully specified by the positions, $\mathbf{r}_i = (x_i, y_i, z_i)$, and the momenta, $\mathbf{p}_i = (p_{x_i}, p_{y_i}, p_{z_i})$, of all the *particles* (the size of these vectors being the only difference between 2D and 3D simulations), which move under the action of the forces that are set up between them. In fact, as discussed in the earlier paper [1], DPD can be considered in terms of a development from molecular dynamics techniques, *via* Brownian dynamics (BD).

The method considers a system of pairwise, additive, symmetric forces between *particles*. The forces being pairwise means that momentum is conserved, *i.e.*, if $\mathbf{P}$ = the total momentum of the system, then

$$\dot{\mathbf{P}} = \sum_i \dot{\mathbf{p}}_i = \sum_i \sum_{j \neq i} \dot{\mathbf{p}}_{ij} = \sum_i \sum_{j<i} (\dot{\mathbf{p}}_{ij} + \dot{\mathbf{p}}_{ji}) = 0. \tag{1}$$

This is a crucial point since it is a pre-requisite, although not in itself sufficient, for the macroscopic behaviour to be hydrodynamic. The transport equation for the momentum density field, along with that for the mass density field, has been derived by Español [13]. Energy is not conserved in the conventional DPD model due to the non-conservative force terms and so there is no transport equation for energy. There are modified versions of DPD [14, 15] which do conserve energy and therefore could be used to study thermal processes in complex fluids. However, the model presented here is the one that is in general use since, to date, DPD has mainly been considered as a tool for studying hydrodynamic processes.

The force between each pair of *particles* is made up of a conservative $\mathbf{F}^C$, a dissipative $\mathbf{F}^D$, and a random $\mathbf{F}^R$ term. The effective force acting on particle i at time t, $\mathbf{F}_i(t)$, is given by

$$\dot{\mathbf{p}}_i = \mathbf{F}_i(t) = \sum_{j \neq i} \mathbf{F}_{ij}^C + \sum_{j \neq i} \mathbf{F}_{ij}^D + \sum_{j \neq i} \mathbf{F}_{ij}^R. \tag{2}$$

The dissipative and random force terms, similar to those of Brownian dynamics, incorporate the effects of Brownian motion into the bigger length scales. However, DPD has the advantage over Brownian dynamics that the solvent is simulated explicitly.

Simulation with mesoscopic particles implies that the relevant hydrodynamic behaviour appears with relatively few particles in comparison to molecular dynamics, and since the scaling of the system is arbitrary, the limits of scale present in MD are irrelevant here. Another major difference between DPD and MD lies in the nature of the interaction potential, described below. There are other mesoscopic simulation techniques: lattice gas automata and lattice Boltzmann dynamics, which might be considered for such simulations. However, the lattice tends to introduce spurious dynamics, especially where complex flows in complex boundaries are required. For this reason, the more flexible off-lattice DPD technique is preferred in such cases.

The three forces in Eq. (2) determine the particle interaction, and are calculated using the following equations.

1. The conservative force

$$\mathbf{F}_{ij}^{C} = \Pi_0 \omega_C(r_{ij})\hat{\mathbf{e}}_{ij}, \tag{3}$$

where $\mathbf{r}_{ij} = \mathbf{r}_i - \mathbf{r}_j$; $r_{ij} = |\mathbf{r}_{ij}|$; $\hat{\mathbf{e}}_{ij} = \mathbf{r}_{ij}/r_{ij}$ and Π_0 is a constant. The value of Π_0 can be calculated from the compressibility of the fluid [16].

2. The dissipative force

$$\mathbf{F}_{ij}^{D} = -\gamma \omega_D(r_{ij})(\hat{\mathbf{e}}_{ij} \cdot \mathbf{p}_{ij})\hat{\mathbf{e}}_{ij}, \tag{4}$$

where $\mathbf{p}_{ij} = \mathbf{p}_i - \mathbf{p}_j$ and γ is a constant.

3. The random force

$$\mathbf{F}_{ij}^{R} = \sigma \omega_R(r_{ij})\hat{\mathbf{e}}_{ij}\zeta_{ij}, \tag{5}$$

where σ is a constant and ζ_{ij} is a random noise term.

The random number ζ_{ij} has zero mean, $\overline{\zeta_{ij}} = 0$, and unit variance. Its values are uncorrelated for different pairs of particles and for different times: $\overline{\zeta_{ij}(t)\zeta_{kl}(t')} = (\delta_{ik}\delta_{jl} + \delta_{il}\delta_{jk})\delta(t - t')$. Note that $\zeta_{ij} = \zeta_{ji}$ is necessary for momentum conservation. Previous studies using DPD have sampled the random number from either a Gaussian or a uniform distribution, in each case with a variance of unity. As part of the work on the earlier paper [1],

both of these distributions were tried with negligible difference between the results. Therefore, due to the lower demand on CPU time, we choose to sample from a uniform distribution. Note also that the parameter σ is the standard deviation of the distribution $\sigma\zeta_{ij}$ in Eq. (5).

The shape of the interaction potential between particles is governed by the weight functions: $\omega_C(r_{ij})$ (Fig. 1), $\omega_D(r_{ij})$ and $\omega_R(r_{ij})$. It is the softness of these interaction potentials that gives DPD its speed up over molecular dynamics, whose interactions use potentials that are high order polynomials of r_{ij}. The soft interaction potential acts as an approximation to the effective potential at mesoscopic length scales [16, 17]. The weight functions all equal zero when the particle separation is greater than the cut-off radius, r_c. Consequently, all particle interactions are local, speeding up the execution of the DPD algorithm. The weight functions $\omega(r)$ are normalised such that

$$\int_V \omega(r)d\mathbf{r} = V/N, \tag{6}$$

where V is the volume of the simulation box and N is the number of particles.

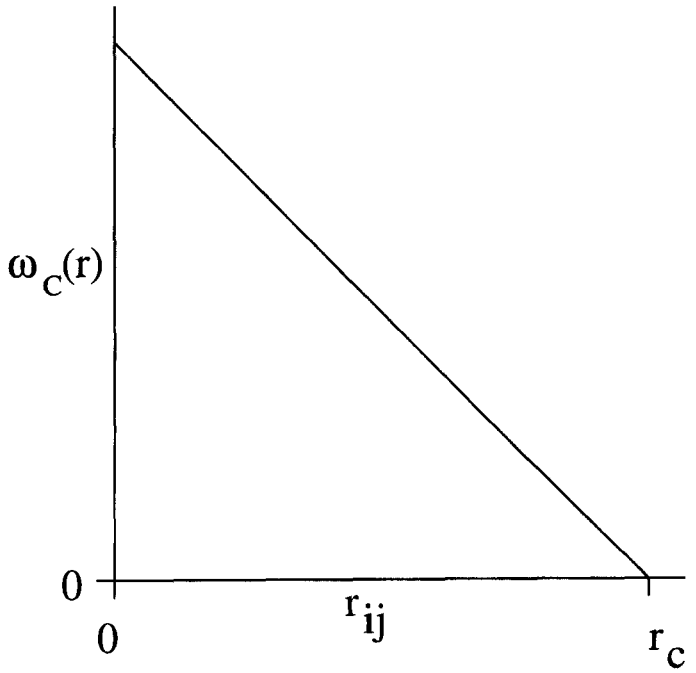

FIGURE 1 The standard weight function.

In early versions of DPD, $\omega_C(r_{ij}) = \omega_D(r_{ij}) = \omega_R(r_{ij})$. However, in 1995 Español and Warren [4] considered the DPD technique as a system of stochastic differential equations and derived the corresponding Fokker-Planck equation. They found that for the system to have the correct equilibrium distribution, the Gibbs canonical ensemble, that the following condition must be satisfied ($\omega_R(r_{ij})$ has been chosen to be the same as $\omega_C(r_{ij})$):

$$\omega_D(r_{ij}) = \omega_R(r_{ij})^2. \tag{7}$$

The equilibrium temperature of the system is then given by a fluctuation-dissipation theorem,

$$k_B T = \sigma^2/2\gamma, \tag{8}$$

where k_B is Boltzmann's constant and T is the system temperature. Note that these results only hold in the limit, $\delta t \to 0$. Marsh and Yeomans [18] have shown that the equilibrium temperature of the system depends strongly on the time step and increases as the time step becomes larger.

As in MD, the instantaneous temperature of the system is obtained from the mean square velocity,

$$3k_B T = \langle \mathbf{p}_i^2/m_i \rangle, \tag{9}$$

where m_i is the mass of particle i and $\langle \cdots \rangle$ indicates an average over all the particles in the simulation.

2.1. The DPD Algorithm

The model progresses in discrete time steps, δt, using an Euler type algorithm. Each time step is comprised of two distinct phases. The first of these is the *interaction* or *collision phase*, where momenta are updated according to the equation,

$$\mathbf{p}_i(t + \delta t) = \mathbf{p}_i(t) + \delta t \sum_{j \neq i} \mathbf{F}_{ij}^C + \delta t \sum_{j \neq i} \mathbf{F}_{ij}^D + \sqrt{\delta t} \sum_{j \neq i} \mathbf{F}_{ij}^R. \tag{10}$$

The $\sqrt{\delta t}$ term is a result of the way the stochastic differential equation is discretised [4, 10].

The second phase, the *propagation phase*, is where the positions of the particles are updated:

$$\mathbf{r}_i(t + \delta t) = \mathbf{r}_i(t) + \frac{\mathbf{p}_i(t + \delta t)}{m_i} \delta t. \tag{11}$$

The units in DPD are dimensionless. All *particles* in our simulations are of equal mass and, for simplicity, the mass of a particle m, as well as its interaction radius r_c, are both set to unity. This means that the force on a particle equals its acceleration and that r_c, being the only length scale in the system, is the unit of length. In the early DPD simulations [3], δt was also conveniently set to unity. However, it has been found [4] that δt must be sufficiently small to ensure the correct equilibrium behaviour in terms of the fluctuation-dissipation theorem. The time step size used must therefore be chosen to give the maximum simulation speed while maintaining accuracy.

2.2. Multiple Phases

Multiple phases are conveniently modelled *via* an additional repulsive force between particles of different phase. For example, to simulate a two-phase system (phase 1 and phase 2, say), we would use the following modified values of Π_0 in Eq. (3):

$$\Pi_0^{11} = \Pi_0^{22} \equiv \Pi_0 \tag{12}$$

and

$$\Pi_0^{12} = \Pi_0(1 + \xi), \tag{13}$$

where the superscripts represent the phases of the pair of particles whose interaction is being considered and $\xi \equiv \xi^{12}$. The same idea can easily be extended to multiple (say n) phases, where we would then have parameters $\xi^{12} \ldots \xi^{1n}$; $\xi^{23} \ldots \xi^{2n}$; $\ldots$; $\xi^{n-1,n}$ to control the various interactions.

A negative value of ξ between solvent and solute particles, where there is less repulsion between particles of different phases than those of the same phase, would produce a good solvent. Conversely, positive ξ means a greater repulsion between particles of different phases, which represents a poor solvent. This technique has been applied with great success to the modelling of binary immiscible fluids [9, 10]. Groot and Warren [16] have directly related the value of ξ to the χ-parameter of Flory-Huggins theory, by applying the condition that the solubility of one phase into the other should be described correctly.

2.3. Structures of Particles

The creation of structures of particles is a useful extension to the basic model. To simulate, for example, a solid wall or particles in suspension,

objects are created. A region of particles is frozen so that the relative positions of the particles within it do not change. This region can either be fixed in space or free to move as a single unit. In the latter case, the momenta of all its comprising particles are summed into a total centre-of-mass linear momentum and an angular momentum, from which the actual propagation can be calculated [5]. In the following simulations, *objects* will be used to represent colloidal particles and solid walls. Previously, *objects* have been successfully used in the simulation of dense colloidal suspensions [11, 12].

Another type of structure is the *polymer*. Here, a bead and spring type model is used to provide an additional force between adjacent particles in the chain. A Fraenkel spring is mainly used:

$$\mathbf{F}_{ij}^{P} = K(r_{ij} - r_{eq})\hat{\mathbf{e}}_{ij}, \tag{14}$$

where K is the spring constant and r_{eq} is the equilibrium spring length.

The work of Schlijper *et al.* [7] on dilute polymer solutions using DPD showed that the static and dynamic scaling relationships are consistent with the Rouse-Zimm model and that both hydrodynamic interaction and excluded volume emerge naturally from the DPD polymer model. This has been confirmed by Kong *et al.* [8], who investigated the effect of solvent quality on the conformation and relaxation of polymers. They also showed that a theta solvent exists for values of ξ in the range 0.0 to 0.05.

3. AN IMPROVED DPD MODEL FOR THE ADSORPTION OF COLLOIDAL PARTICLES ONTO A POLYMER COATED SURFACE

Although the model used in [1] achieved good results, it also showed some weaknesses. One unrealistic aspect of that series of simulations was the presence of a depletion layer near to the walls, caused by the high density of particles inside them (see Fig. 2). Although a depletion layer may be physically realistic at the microscopic level, at the coarse-grained level of a DPD simulation, the numerical resolution is not sufficient for such a layer to be justified. This may lead to such problems as the colloidal particles getting trapped close to the back wall by the imbalance of forces that this layer creates. This particular effect can be spotted and bypassed by reducing the density of the particles in the solvent wall, so eliminating the associated depletion layer. However, the effect of the depletion layer at the colloidal particle wall may be more significant. One factor is that the calculation and

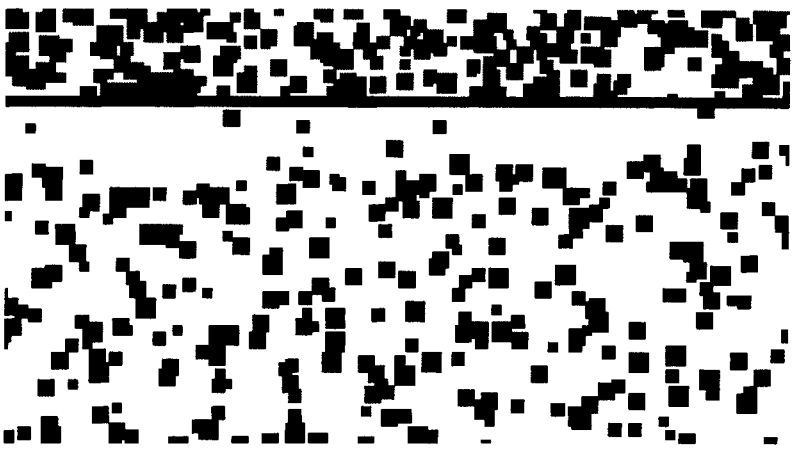

FIGURE 2 The depletion layer.

control of the force between a colloidal particle and the wall is complicated by the opposing effects of the high density of particles in the wall and the absence of particles in the depletion layer. Ideally, the wall would be at the same density as the solvent, eliminating both of these undesirable effects. There is also the fact that the extra particles required to produce a high density wall significantly increase the demand on CPU time. However, simply reducing the density of the wall to that of the solvent would make the degree of penetration by the polymers and the solvent unacceptable. Even at three times the solvent density, a slight amount of wall crossing did take place.

A satisfactory answer was found by introducing a *virtual wall* into the model. This idea has been adopted from work currently being undertaken by Charles Manke at Wayne State University. The wall provides an invisible barrier that simply reflects back any particle that tries to cross it. Two such barriers are used – one at each side of the wall, as shown in Figure 3. Inside the wall is a layer of solvent particles and a layer of particles similar to those in a colloidal particle, as before, although this time they are at the same density as the solvent. The particles in the wall are, of course, still frozen in space. As in [1], the soot solvency $\xi = 0.3$. Despite this additional repulsion that exists between the colloidal particle wall and the solvent particles over that between just solvent particles, there is no discernible depletion layer present with this virtual wall model (see Fig. 4). In §4, variation on this wall model is also considered.

It is now much easier to accurately calculate the force between a colloidal particle and the attractive wall, since it can now be correctly assumed that

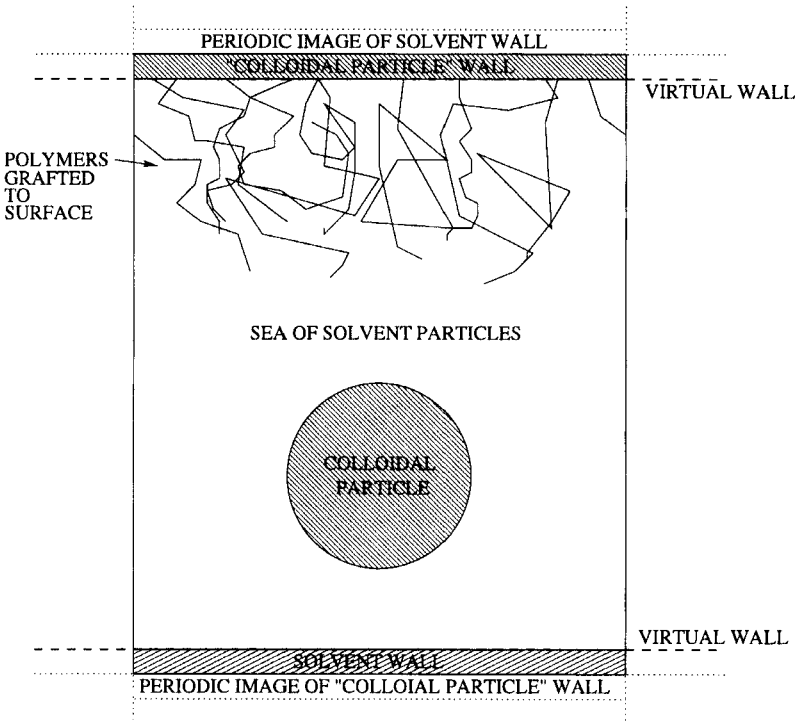

FIGURE 3 The DPD model for the adsorption of colloidal particles.

FIGURE 4 No depletion layer with virtual wall.

the solvent density is, on average, equal throughout the solvent. The calculation was made by considering the net force on a single DPD particle, of the same phase as the colloidal particle, as it approaches the wall and then integrating over the whole colloidal particle. Figure 5 shows how this force varies with distance from the wall. A negative value for the force indicates that it is attractive. This net attractive force is directly due to the greater repulsion on the colloidal particle from the solvent than the wall. For our parameter values, the particle-wall attraction is equivalent to a potential with a well-depth o $6.1\,k_BT$. We could adjust this directly by altering the value of ξ between the solvent and wall using *well depth* $= 0.0761\xi r_{cp} - 0.0114\xi$, where r_{cp} is the radius of the colloidal particle. However, if we increase it too much we risk re-introducing the depletion layer. The above value is sufficient for the purposes of our simulation.

3.1. Simulation Results

Apart from the modifications due to the introduction of the virtual wall, the simulation details were largely unchanged from those of [1]. It was found that, for a given polymer density and length, with a virtual wall present the polymers had a greater radius of gyration than without, *i.e.*, they stretched further away from the wall. This meant that the colloidal particle had to be

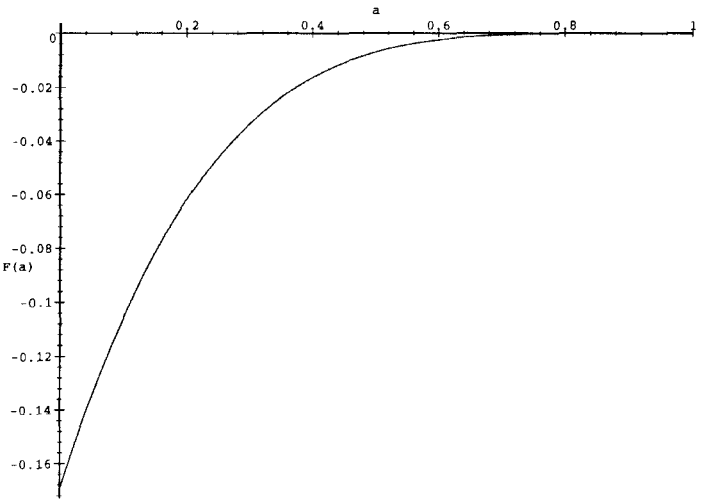

FIGURE 5 The force between a colloidal particle and the wall for the parameter values in our simulations: $r_c = 1$, $\Pi_0 = 1/3$, $n = 3$, $r_{cp} = 1.491$ and $\xi = 0.3$.

larger to maintain the same relative polymer length, which in turn results in a greater relative polymer surface density. The presence of the virtual wall, in other words, made it more difficult for the colloidal particle to absorb for a given configuration.

A new standard simulation configuration was adopted, from which individual parameters could be varied and then the simulation results compared:

- number of colloidal particles = 1
- relative colloidal particle density = 2.35
- relative polymer length = 1.0
- relative polymer surface density = 1.556
- polymer solvency = 0.0
- temperature, $3k_BT = 0.005$.

The relative polymer surface density is lower than in the previous simulations (where it was 1.586) to compensate for the greater polymer length and colloidal particle size. The virtual wall makes the relationship between the polymer length and density more realistic. Note that these simulations are conducted at $\delta t = 1$ since it was shown in [1] that for this type of simulation, such a value gives the same results, allowing for statistical variations, as values as low as $\delta t = 0.05$. It was also shown that there is no trend in the behaviour of the simulations as the time step is reduced.

3.2. Variation in the Relative Polymer Length

The relative polymer length was varied and the results are shown in Table I. The column headed '*y*/*n*' indicates whether or not adsorption has taken place – '*y*' denoting yes, the particle has adsorbed and '*n*', no, the particle has not adsorbed. The time taken for the particle to adsorb is also given in dimensionless DPD units. Since the time step size $\delta t = 1$, the time taken is the same as the number of time steps. The 'closest approach' column gives the closest approach of the edge of the colloidal particle to the wall over the course of the simulation, a negative value indicating that the edge of the

TABLE I The effect of the relative polymer length on particle adsorption

		Adsorption		
Rel. poly. length	*Rel. monomer dens.*	*y/n*	*Time taken*	*Closest approach*
0.400	1.56	y	6,310	−0.28
1.0	4.28	y	198,410	−0.10
1.942	4.51	n	> 400,000	4.12

particle has crossed over the wall. Note that this is possible since the wall's reflective behaviour applies only to the solvent and polymer particles and not to objects.

The results clearly show a trend that the longer the polymer is relative to the colloidal particle radius, the longer the time taken for it to adsorb. They also indicate that this effect may be partly due to the increase in relative monomer density with relative polymer length. As in all these simulations, all the other variables are held constant at their standard values. This trend is in agreement with the results of [1]:

3.3. Variation in the Relative Polymer Surface Density

Table II, as in [1], shows the colloidal particle being less likely to adsorb as the relative polymer surface density, and hence the relative monomer density, is increased.

3.4. Variation in the Location of the Polymers

A couple of variations were tried on one of the previous set of results, the case where the relative polymer surface density is 1.706 was repeated with the polymers attached to the colloidal particle, as well as and then instead of, the wall. The polymers were attached to the particle at approximately the same surface density as they were to the wall. However, Table III shows that the same relative surface density leads to a much lower relative monomer density around the colloidal particle. Since the monomer density is defined as the average density of monomers within a distance of $2r_c$ of the grafting surface, chosen as the most critical region in preventing adsorption, the different geometries of the wall and particle lead directly to a difference in relative monomer density.

For both the particle only and the particle plus wall cases the colloidal particle did not adsorb, although there is a significant difference in the closest approach of the colloidal particle to the wall, as shown in Table III. Despite

TABLE II The effect of the relative polymer surface density on particle adsorption

		Adsorption		
Rel. poly. surface dens.	*Rel. monomer dens.*	*y/n*	*Time taken*	*Closest approach*
1.251	3.76	y	8,050	−0.33
1.556	4.28	y	198,410	−0.10
1.706	4.52	y	98,150	−0.11
2.227	5.31	n	> 400,000	1.86

TABLE III The effect of the location of the polymers on particle adsorption

Poly. location	*Rel. poly. surface dens.*	*Rel. mono. dens.*	*Adsorption*		*Closest approach*
			y/n	*Time taken*	
wall only	1.706	4.52	y	98,150	−0.11
particle only	1.671	1.60	n	> 400,000	1.44
wall and particle	as above	as above	n	> 400,000	4.28

having roughly equal relative polymer surface densities and a much lower relative monomer density, the polymers located on the colloidal particle rather than the wall are more effective at preventing particle adsorption. This is because it is not actually the surface density that is important as the colloidal particle approaches the wall but the number of polymer particles which are interacting with the wall. A spherical surface is better than a flat one at the same surface density because the polymers are all concentrated close to the same region of the wall, allowing many more polymers to interact with it at any one time. As expected, layers of polymers on both surfaces make it much more difficult for the colloidal particle to approach the wall.

3.5. Variation in the Polymer Solvency

As in the earlier simulations [1], the neutral and poor solvents allowed adsorption to take place while the good solvent did not (see Tab. IV). Again, the effectiveness of the barrier in the good solvent case appears to be due to more than merely the associated increase in the relative polymer length (*cf.* Tab. I) and occurs despite the reduction in the relative monomer density. This is because the polymers prefer the solvent to the colloidal particle due to the lower repulsion and so the colloidal particle is forced back. If the relative polymer length was increased on its own, the neutral solvency would mean that the polymers would be equally attracted to the solvent and colloidal particle, which would allow the colloidal particle to penetrate into the polymers much more easily.

TABLE IV The effect of the polymer solvency on particle adsorption

Poly. solvency	*Rel. poly. length*	*Rel. monomer dens.*	*Adsorption*		*Closest approach*
			y/n	*Time taken*	
0.3	0.832	6.16	y	108,960	−0.10
0.0	1.0	4.28	y	198,410	−0.10
−0.3	1.354	2.44	n	> 400,000	5.28

TABLE V The effect of the system temperature on particle adsorption

System temp.	*Rel. poly. length*	*Rel. monomer dens.*	*Adsorption*		*Closest approach*
			y/n	*Time taken*	
0.0025	0.985	4.43	y	349,750	0.09
0.005	1.0	4.28	y	198,410	−0.10
0.1	1.022	4.14	n	> 400,000	2.06

3.6. Variation in the System Temperature

The system temperature was varied using Eq. (8). It is clear from Table V that more simulations are necessary before any trend can be spotted in the behaviour. It is interesting, although perhaps not significant, that as in [1], both doubling and halving the temperature from the standard value seems to make adsorption more difficult. However, the results do show how the relative polymer length increases with temperature while the relative monomer density decreases.

3.7. Summary

This series of simulations has produced results that agree very well with both physical reasoning and previous simulation results [1]. They have demonstrated that particle adsorption becomes less likely as the size of the polymers relative to the colloidal particle increases and as the density of the polymers increases. They have shown the effectiveness of good polymer solvency at preventing adsorption. The effects of temperature require further investigation. They have also demonstrated, quite predictably, how adsorption is much less likely when both the colloidal particles under consideration have an attached polymer layer.

This new model for the colloidal particle adsorption process has been more realistic than previous versions in that the depletion layers near to the wall are no longer present. Although this improvement has had no qualitative effect on the results for this series of simulations, it has led to quantitative changes and has also allowed us to predict the force between a colloidal particle and the wall (see Fig. 5). The greater radius of gyration for the polymers in a given configuration has altered the relationship between the different simulation parameters. As it is the ratios between different parameters that allows the system to be scaled to realistic systems, it can be concluded that the new model should provide more realistic, and hence useful, data.

The results given here have been from single simulation runs and are intended to demonstrate qualitatively the effects on the adsorption process of varying certain fundamental parameters. Multiple runs would be necessary before an accurate quantitative analysis of the behaviour and the potential between the particle and the polymer coated wall could be carried out.

4. THE PROCESS OF POLYMER ADSORPTION

In the colloidal particle simulations which have been attempted up until now, the surface has its polymer layer physically grafted on. This is adequate for the investigation of the effect on particle adsorption of varying some fundamental parameters but a more complete approach is to allow the polymer layer to reach a natural equilibrium. For example, in the simulation of a soot-oil-dispersant system, the oil will contain a certain concentration of dispersant. The soot will enter the oil, presumably at a rate slow enough to be able to assume that the concentration of soot in the oil at any given time is constant, relative to the time scales in which dispersant adsorption and soot agglomeration occur. This oil-dispersant-soot system will naturally attempt to move towards some kind of an equilibrium state, which means that the concentration of dispersant (polymers) on the surface of a colloidal particle is also likely to move towards some equilibrium value. This is very different from the way this concentration was fixed in the previous simulations.

In order to investigate such an equilibrium state, a number of simulations were carried out in which a given concentration of polymers was distributed randomly throughout the solvent. The rate of adsorption was investigated and the equilibrium concentration of polymers adsorbed on to the wall was observed. The dependence of these two factors on the initial concentration of polymers in solution was also looked at. These experiments were conducted for two different wall models: the *solid wall* and the *porous wall*. These are described in the next section. Simulations were also conducted in which a colloidal particle was introduced into the solvent. This was tried for both the colloidal particle being added to the equilibrium state of the solution and, perhaps more realistically, with it being added at the outset of the simulation when the polymers are distributed randomly. The effect of the presence of the colloidal particle on the equilibrium that is reached was then observed.

4.1. The Solid Wall and Porous Wall Models

The series of experiments in the previous section used a *solid wall* model. The surface of this wall is perfectly flat and coincides with the reflective

virtual wall. Free polymers could adsorb onto such a wall by being trapped onto its surface by the various interparticle forces. An alternative to this approach is the *porous wall* model. With this configuration, the virtual wall is initially set up, exactly as before. However, a further thin layer (thickness = 0.5) of colloidal particle wall is then frozen in place on top of the virtual wall. This layer is at the same density as the rest of the wall. This new layer makes the first section of the wall porous so that free polymers can now adsorb by penetrating slightly into the wall's surface. Whether such an attachment would be more permanent and whether or not a porous wall would allow the adsorption of a greater number of polymers is something that the following simulations will attempt to determine.

4.2. The Model Parameters

Several parameter values were changed from those that had been used in previous simulations. The length of the time step, δt, was reduced from 1 to 0.25. This ensured the accuracy of the results. The nature of the polymers was also altered in order to greatly reduce polymer crossing. The spring constant K was increased from 0.25 to 1.0, making the springs stiffer, and the equilibrium spring length r_{eq} was reduced from 0.85 to 0.65, making the polymers shorter and denser. A full description of how the changes in these two parameters reduce the frequency of polymer crossing can be found §6.

The size of simulation box used in these simulations was $10 \times 12.5 \times 10$, the 12.5 being the direction perpendicular to the wall. As the polymers were adjusted to a higher density, the density of the solvent was also increased to try to keep the densities of the solvent and monomers approximately equal. In previous simulations, a density of 3 had been used, which for this size of box would mean a total of 3750 particles. To take into account the increase in the polymer density, the overall density (and hence number of particles) was increased by a fraction equal to the proportion by which the equilibrium separation of the polymer beads was reduced, *i.e.*,

$$N' = N\left(1 + \frac{r_{eq} - r'_{eq}}{r_{eq}}\right) \tag{15}$$

where N is the number of particles and r_{eq} is the equilibrium spring length with the old spring model. N' is the number of particles after adjustment for the new shorter spring length, r'_{eq}. Given that $N = 3750$, $r_{eq} = 0.85$ and $r'_{eq} = 0.65$, a value of $N' = 4632$ was used in these simulations.

Some important parameter choices for these simulations concern the nature of the polymers. The polymers were simulated as diblock copolymers, where one part of the polymer, the *head*, was attracted to the colloidal particle wall (by nature of the head-colloidal particle repulsion being less than the head-solvent repulsion) and the other part, the *tail* was made up of particles similar in nature to the solvent. The relationship between the different types of particle in the simulations is complex and is summarised in Table VI. The table gives the values of the interphase repulsion parameter ξ between the various types of particle, remembering that a negative value indicates an attraction and a positive value a repulsion, relative to the neutral interaction, $\xi = 0$. Note that these values differ from those used in the simulations of particle adsorption.

Solvent particles and those in the polymer tail are actually the same phase but have been separated in the table to make the various interactions clearer. It can be seen that there is a repulsion between the tail and the head of the polymer, keeping the two parts of the polymer separate. There is also a repulsion between the head of the polymer and the solvent. This encourages the polymers to form micelles within the solvent, where the heads cluster together in small groups. This is a physically realistic behaviour. There is a net attraction between the colloidal particle wall and the polymer head which leads to the head adsorbing onto the wall. This is a characteristic required of a dispersant. The polymer tail is neutral with respect to the solvent, equivalent to the *polymer solvency* being neutral in the particle adsorption simulations. Its effect on the polymer adsorption process will be assumed to be insignificant when compared to the characteristics of the head. The polymer tail and the colloidal particle wall repel, since only the head should adsorb. Finally, the solvent and the colloidal particles (including the wall) repel. This encourages any colloidal particles present to agglomerate with each other and/or to adsorb onto the wall.

The length of the polymer and the relative sizes of the head and tail are also important. Initially both sections of the polymer were set to be five beads long. Absorption behaviour was observed but results were a little

TABLE VI The values of the interphase repulsion parameter ξ

	Polymer			
	Head	*Tail*	*Solvent*	*Colloidal particle wall*
head	0.0	0.3	0.3	−0.3
tail	0.3	0.0	0.0	0.3
solvent	0.3	0.0	0.0	0.3
colloidal particle wall	−0.3	0.3	0.3	0.0

erratic, so that a large number of simulations would have been required to obtain consistency. We found that better results were obtained by using a short head and a long tail, which is also a more realistic arrangement. For this reason, a head of length two beads and a tail of five beads was chosen. Adsorption behaviour was a lot smoother and more consistent. A presentation of the results follows.

4.3. Polymer Adsorption Simulations

Simulations were carried out with 50, 75, 100, 150 and 200 polymers. They were initially randomly distributed throughout the solvent. The simulations were run for a maximum of 3 million time steps each. The same simulations were done for both the solid and porous wall models. Figures 6 and 7 show the number of polymers adsorbed onto the wall over time for the solid and porous wall cases respectively.

The two graphs are very similar. They both show that the rate of adsorption increases with the number of free polymers. They also show that in the simulations with 50 and 75 polymers, all the polymers adsorb onto the

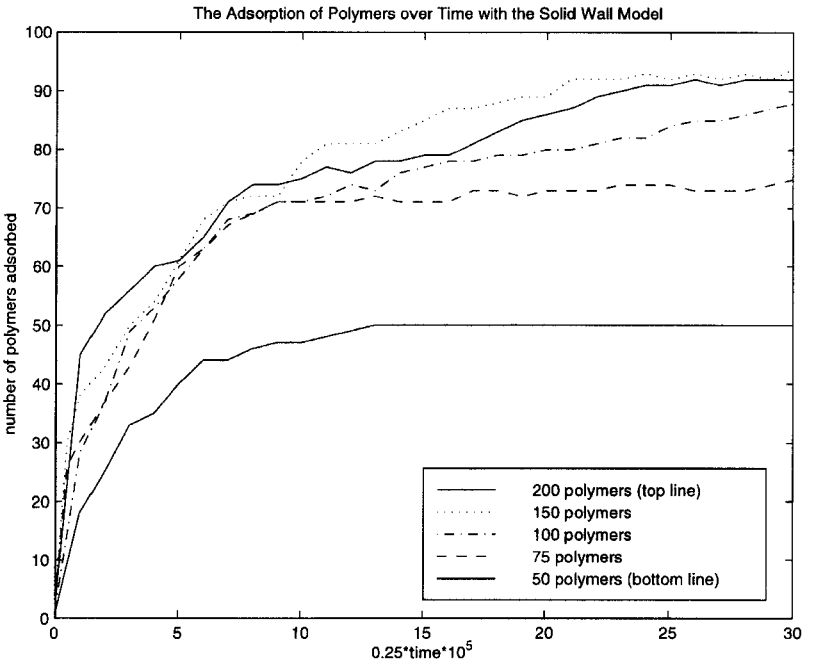

FIGURE 6 The Adsorption of polymers over time with the solid wall model.

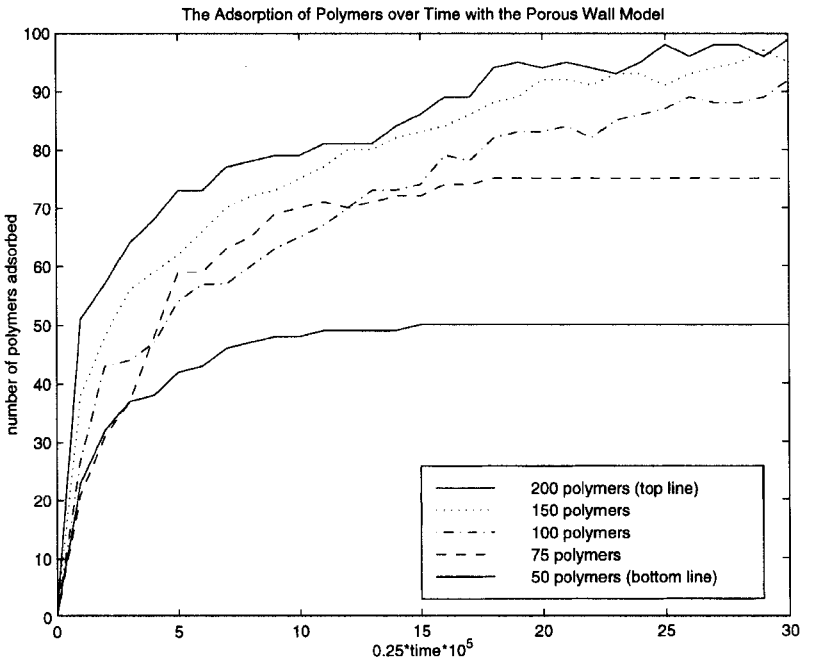

FIGURE 7 The Adsorption of polymers over time with the porous wall model.

wall, while this is not the case for the simulations with 100, 150 or 200 polymers. The adsorption curves for these cases indicate a maximum number of polymers that can adsorb onto the wall that the simulation is asymptotically moving towards. This is perhaps more clearly illustrated by Figures 8 and 9. The final numbers of adsorbed polymers shown in these figures can be assumed to be very close to the equilibrium value.

The maximum number of polymers that can adsorb onto the solid wall is observed to be around 94, while the porous wall can hold slightly more at around 99. The consistency of these results over time indicates that this difference is significant, although slight fluctuations are possible, as can be seen in Figure 8. This difference in the polymer adsorption limit is because the polymer head penetrates inside the porous wall rather than having to take up surface positions as with the solid wall. The difference is only slight because the polymer head is only two beads long in these simulations. The difference is expected to be more significant with a larger head.

During the simulations, the free polymers quickly form a number of micelles (for reasons given in the previous section). These structures are not

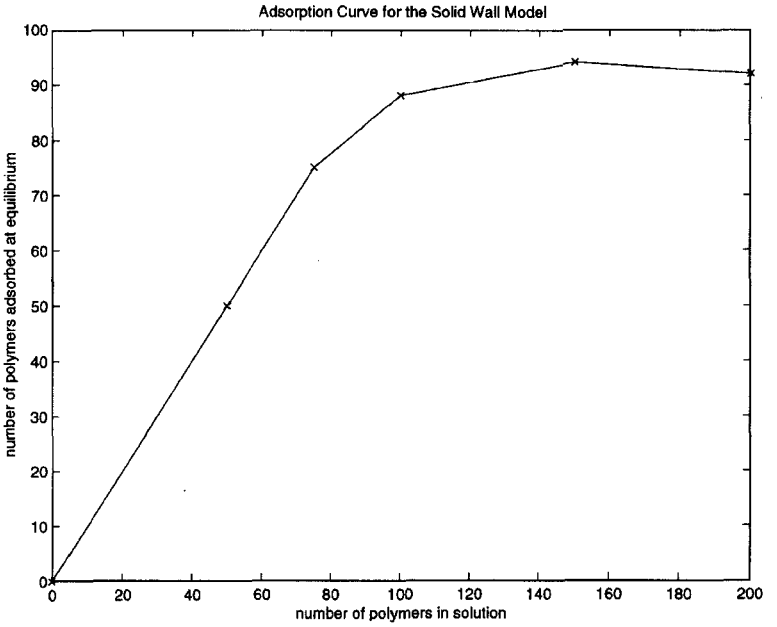

FIGURE 8 The final number of polymers adsorbed with the solid wall model.

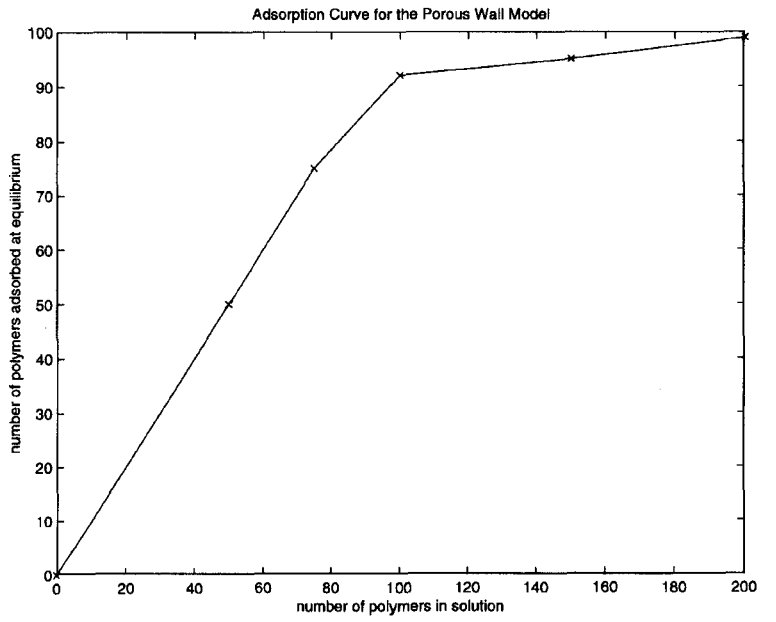

FIGURE 9 The final number of polymers adsorbed with the porous wall model.

particularly stable and frequently break up, reform and merge with one another during the course of a simulation. They have little effect on the adsorption process, as the attraction of the polymer heads to the wall is a lot stronger. The graphs (Figs. 6 and 7) clearly show that polymers can leave as well as join the wall. This is evident when the wall is close to its maximum polymer count, at which time the crowding of polymers on the wall can lead to repulsive forces sufficient to dislodge a polymer. However, it will usually be replaced at some time and an equilibrium maintained. Figures 10 to 12 show, respectively, the state of the simulation of 100 polymers with a solid wall at the start of the simulation, after 10^5 time steps and after 3 million

FIGURE 10 The initial configuration for the simulation of 100 polymers with a solid wall.

FIGURE 11 The state of the simulation of 100 polymers with a solid wall after 10^5 time steps.

time steps, when it is close to an equilibrium configuration. Figure 13 shows the equivalent porous model simulation after 3 million time steps.

4.4. Polymer Adsorption Simulations with a Colloidal Particle

Simulations were also conducted with a colloidal particle present. These were carried out using the solid wall model with 75 polymers: a case in which all the polymers adsorbed in the previous simulations. This configuration

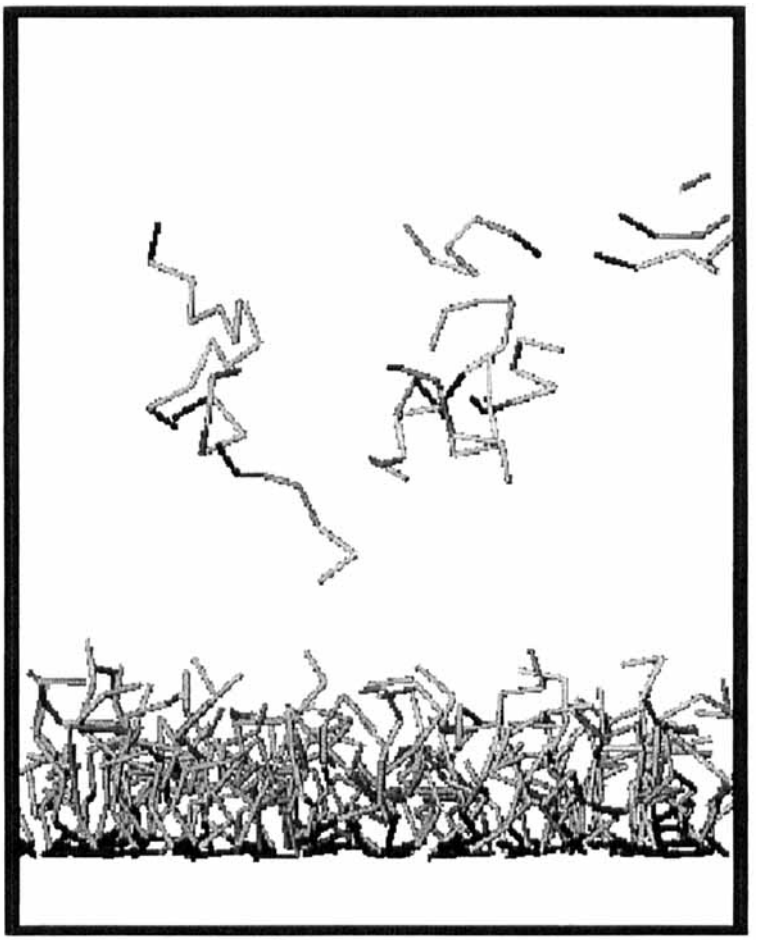

FIGURE 12 The state of the simulation of 100 polymers with a solid wall after 3 million time steps.

was chosen to allow some comparison to be made with the particle adsorption simulations. The first experiment was to add the colloidal particle to the final equilibrium configuration reached in the last set of simulations. The radius of gyration of the adsorbed polymers was calculated to be 0.85. This is less than when 75 polymers had been simulated in the particle adsorption simulations of §3 because of the reduction in the equilibrium spring length. The colloidal particle radius was also set to 0.85 to give a *relative polymer length* of 1 and a *relative polymer surface density* of 0.54. Based on the results

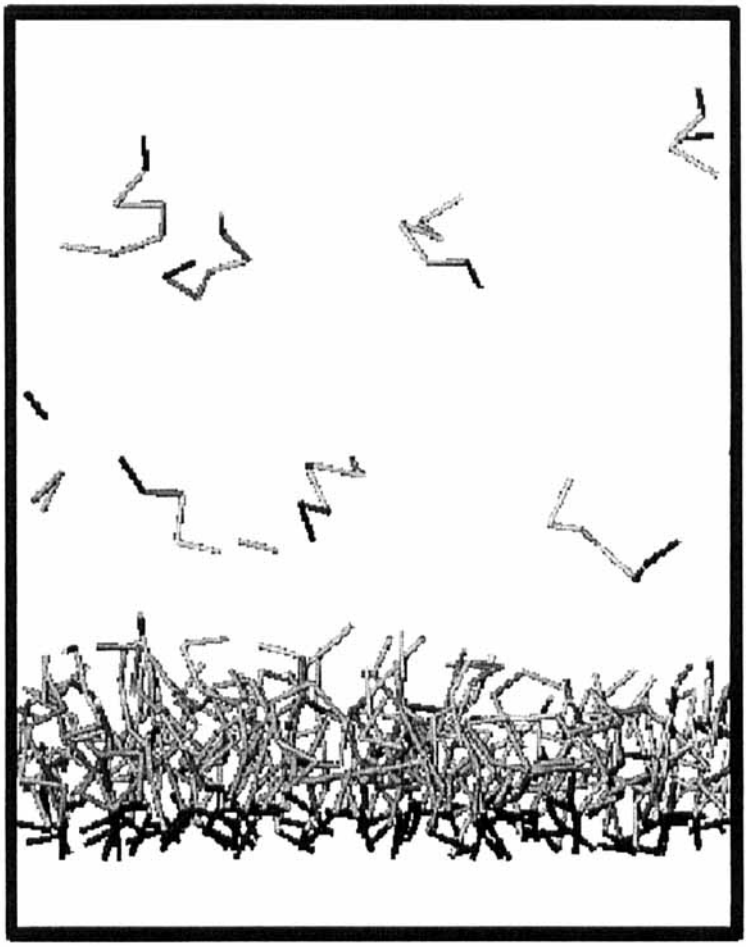

FIGURE 13 The state of the simulation of 100 polymers with a porous wall after 3 million time steps.

of §3.3, the colloidal particle might have been expected to adsorb easily at this low value of *relative polymer surface density* but after 1 million time steps showed no sign of doing so. The reason is that there is now a repulsion between the colloidal particle and the polymer tail, whereas in the previous simulation studies of particle adsorption their interaction was neutral. The polymer tails which cover the wall form an excellent repulsive barrier to the colloidal particle. However, during the simulation one polymer did manage to leave the wall and attach itself to the colloidal particle.

A simulation was also carried out with a colloidal particle of radius 0.85 introduced at the start of the simulation, after the 75 polymers had been initialised into random locations throughout the solvent. This was perhaps more realistic, with an equilibrium being arrived at between the polymers on the wall and the polymers attached to the colloidal particle. Particle adsorption was a possibility but did not occur during the 3 million time steps of the simulation and was unlikely once the polymer barriers had moved into position. The distribution of polymers over the simulation amongst the wall, the colloidal particle and being free in the solvent (usually in micelles) is given in Figure 14. The graph shows how the system moves towards an equilibrium configuration.

The number of free polymers falls off rapidly after the start of the simulation and after about half a million time steps, their number fluctuates just above zero. This is because the wall and colloidal particle are more attractive to polymer heads than micelle structures are. Therefore it is more interesting to see how the polymers distribute themselves between the wall and colloidal particle. The curve of polymer adsorption onto the wall is

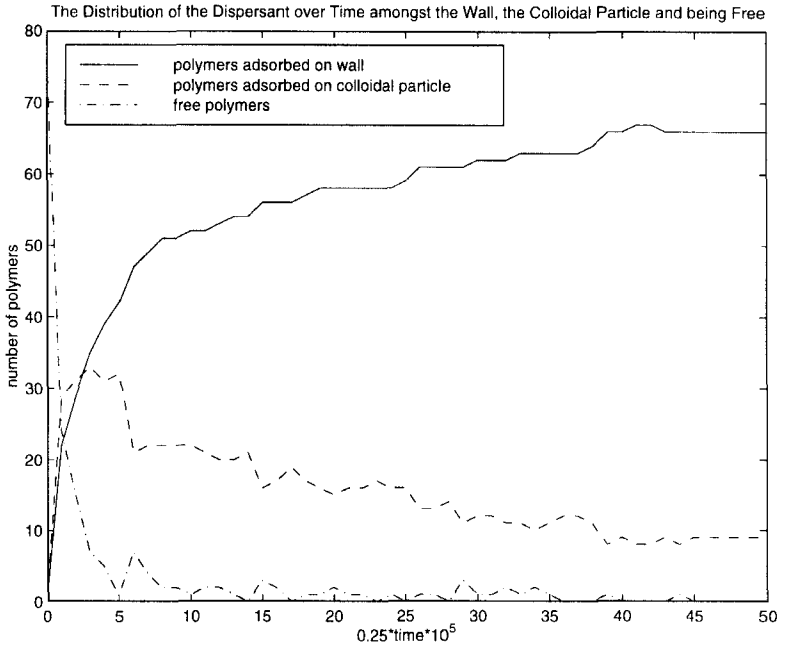

FIGURE 14 The distribution of polymers over time between being attached to the wall, attachment to the colloidal particle and being free.

similar to previous results but appears a little smoother and the equilibrium number of polymers is obviously less due to the competition from the colloidal particle. Initially, the colloidal particle attracts more polymers due to its greater accessibility but most of these are only held very weakly and may be better described as associated with the colloidal particle rather than adsorbed onto it. The final distribution has 66 polymers on the wall and 9 on the colloidal particle. This arrangement appears to be a stable one.

It might be predicted that the final distribution would approximate the ratio between the two surface areas. Since the respective surface areas of the wall and colloidal particle are 100 and about 9.1 respectively, this would mean that the wall would be expected to contain $100/9.1 \approx 11$ times as may polymers as the colloidal particle. Instead, it contains only $66/9 \approx 7.3$ times the number. However, we know from previous results that the wall can potentially hold far more than 66 polymers. At the same time, the decrease in the number of polymers on the colloidal particle over time in Figure 14 suggests that the colloidal particle may have settled down to the maximum number of polymers that it can hold on to. It seems that the colloidal particle's location in the middle of the polymers was better at attracting the polymers than the wall, at the edge, and so it could maximise its polymer coverage where the wall could not. Another interesting piece of evidence supporting this idea is given by multiplying the number of polymers on the colloidal particle by the ratio of its surface area to that of the wall, *i.e.*, $9 \times 11 = 99$. The answer, 99, equals the maximum number of polymers adsorbed onto the porous wall in the previous experiments (note that this is the correct comparison because the surface of the colloidal particle is also porous). This suggests that the maximum number of polymers adsorbed onto a surface at equilibrium is directly proportional to the area of that surface, and that curvature of the surface has little affect on this. Simulations without a wall present would be a useful way to explore this idea. Another useful follow-up to the wall plus colloidal particle adsorption simulation would be to repeat it using a porous wall and with excess polymers so that both surfaces are similar in nature and can maximise their coverage. This should help to confirm the above conjecture.

4.5. Summary

Simulations have been carried out in which a number of polymers is initially randomly distributed throughout the solvent, before being allowed to reach a natural equilibrium. This was done for two alternative wall models: the

solid wall and the *porous wall.* The simulations have shown that the rate of polymer adsorption onto the wall increases with the concentration of polymers in solution. They also show that the number of adsorbed polymers tends toward some maximum value, given that an excess number of polymers is available. This value is slightly greater with a porous rather than a solid wall because the polymer head can penetrate the wall rather than having to occupy surface positions. The simulations also reproduced phenomena such as micelle formation and polymers leaving as well as joining the colloidal particle wall.

When a colloidal particle was added to the equilibrium configuration of one of the above simulations it did not adsorb because of the repulsion between the colloidal particle and the polymer tails forming a barrier. This force had not been present in the particle adsorption simulations of [1] or §3. In the case where the colloidal particle was added at the start of the simulation, when the polymers were distributed randomly, an equilibrium was reached between the number of polymers adsorbed on the wall and on the colloidal particle. The colloidal particle's location allowed it greater access to the polymers, so it could maximise its polymer coverage, where the wall could not. The figures for maximum coverage of the colloidal particle and of the wall, which was obtained earlier, indicate that the maximum concentration of polymers that can adsorb onto a surface at equilibrium is directly proportional to the area of that surface, and that curvature has little affect on this. Further data is required before this can be confirmed.

5. AN INVESTIGATION INTO POLYMER CROSSING

The chain conformation plays an important role in dense polymer systems, such as polymer melts, cross-linked networks, and dense polymer brushes, like that used in the particle adsorption simulations. One important property of these systems is that the chains cannot move through each other. This fundamental property must be taken into account when such systems are simulated because it plays a dominant role in the dynamical and relaxational behaviour. In contrast to small molecules, the motion of a polymer chain in a dense system is more complex than simply random diffusion, at least over length scales smaller than its own size. Indeed, this property of polymers results in entanglement effects in dense systems.

Therefore, when such dense polymer systems are simulated, such as the polymer brush used in our particle adsorption simulations, we expect such entanglement effects among the polymers. This provides the motivation for

the following study: to find out to what extent the polymers entangle in the simulations of polymer brushes, by studying the extent of any polymer crossing. We will then be able to determine whether this aspect of the simulations is suitably realistic and, if it is shown not to be, to make the necessary changes to the model.

5.1. The Polymer Crossing Model

In our simulations polymers are represented using a bead and spring type model (see §2.3), where polymers consist of a series of beads and each pair of adjacent beads are connected by a Fraenkel spring. The springs are characterised by two parameters: spring length r_{eq} and spring constant K. Note that the Fraenkel spring used in the model is essentially a virtual spring, since there is no "physical" mechanism between the beads to prevent the polymers from crossing one another. This study will measure the intensity of any polymer crossing and then consider ways of reducing it. To do this, a new model, consisting of interlocked polymer rings, has been introduced, as shown in Figure 15. A polymer ring can be viewed as a linear polymer joined end to end.

We investigated polymer crossing by considering the two spring parameters: the spring constant and the spring length. This study looks at how long two initially interlocked polymer rings remain interlocked (or in other words, how long it takes them to separate) as these parameters are varied. This time is used as an indication of the frequency of polymer crossing, *i.e.*, the longer they hold together, the less frequent the polymer crossing.

5.2. Simulation Results

In order to approximately determine the time at which two interlocked chains separate, the distance between the two mass centres of the polymer rings was calculated and plotted against time. A typical curve is illustrated in Figure 16, where two 8-bead rings are being simulated with $K = 1.0$ and $r_{eq} = 0.65$. A large jump in distance can be seen when the two initially interlocked polymer rings separate. Accordingly, the jump point, denoted by the dashed line in the figure, is regarded as the time taken to break the interlocking. Simulations were conducted at several parameter sets of K and r_{eq}.

Figure 17 shows the results, with two curves for the two different spring lengths used. The X-axis is the spring constant and the Y-axis is the time needed to break the interlocked polymer rings. The curves show that the stronger and the shorter the springs, the longer the two interlocked polymers hold together, *i.e.*, the less the polymer crossing. This finding makes physical

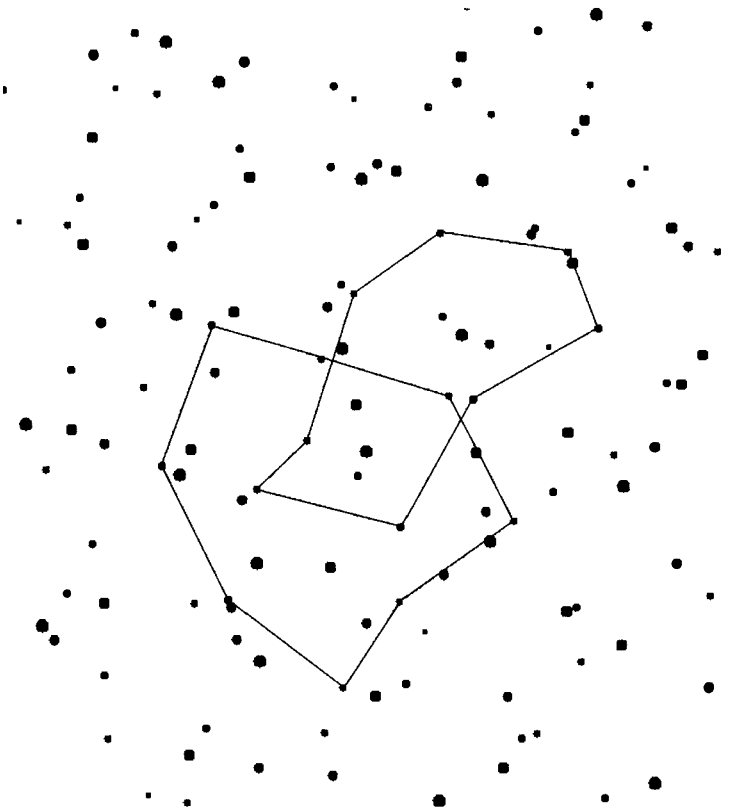

FIGURE 15 The polymer crossing model: two interlocked polymer rings.

sense because, with both shorter and stronger springs, the polymer beads are closer together. Therefore, the results show that more closely connected beads result in less polymer crossing.

The conventional parameter set of $K = 0.25$ and $r_{eq} = 0.85$ [6–8] has not been included in the figure because the jump point cannot be observed for these values. This indicates that for this case polymer crossing is so severe that one polymer hardly even senses the presence of the other. It should also be noted that as long as the Fraenkel spring-bead model is used to represent polymers, a certain amount of polymer crossing is inevitable, no matter what parameter are used. Our aim is to limit it so that simulation results are not adversely affected.

The time step size also has an impact on polymer crossing. A reasonable reduction in time step size leads to slightly less polymer crossing, although the effect is not as significant as with the parameters, K and r_{eq}.

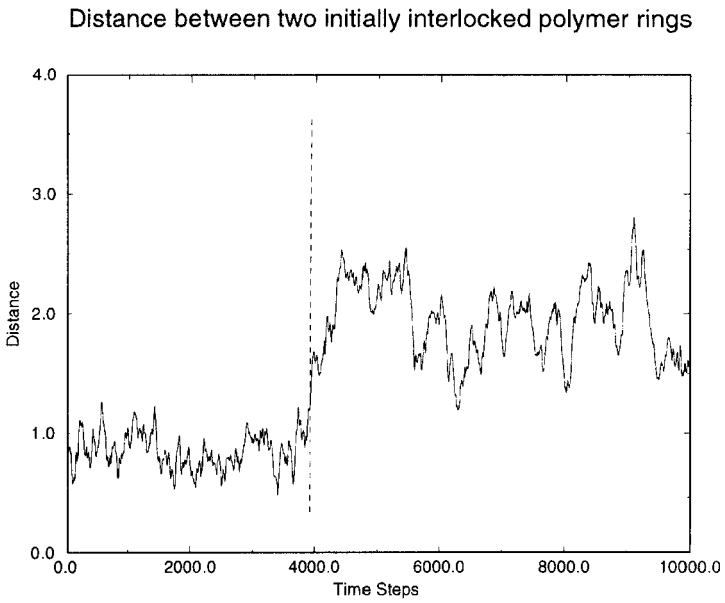

FIGURE 16 The Separation over time of two 8-bead polymer rings with $K = 1.0$ and $r_{eq} = 0.65$.

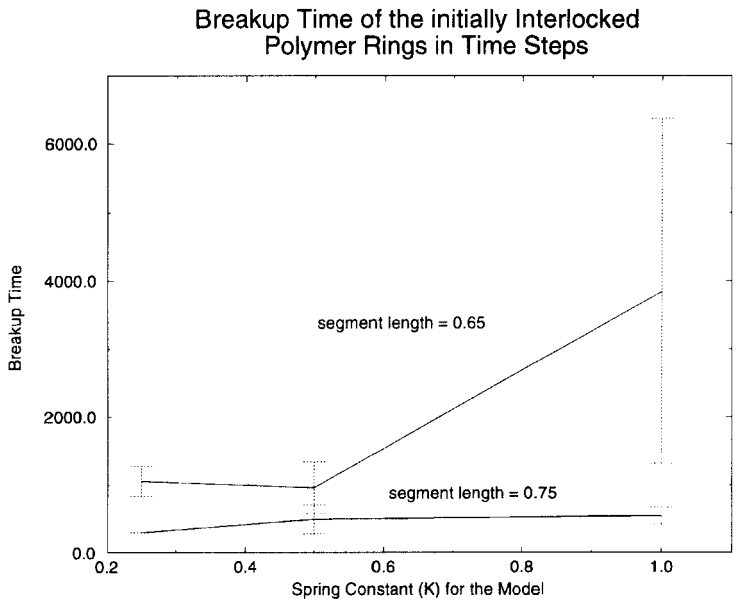

FIGURE 17 The Separation times for different polymer configurations.

The results suggest that the parameter set $K = 1.0$ and $r_{eq} = 0.65$ is preferable to the conventional values ($K = 0.25$ and $r_{eq} = 0.85$) when dense polymer systems are involved. By reducing the extent of polymer crossing, the simulations become more realistic. This is supported by the results of the following section.

5.3. The Effect of Polymer Crossing on the Adsorption of Colloidal Particles onto a Polymer Coated Surface

Following the study of polymer crossing, a follow-up investigation was conducted to find out how a reduction in the extent of crossing in the polymer layer affects the particle adsorption results obtained previously. Two different types of Fraenkel springs were used in these simulations. The first is the *crossing spring*, defined by the conventional parameters set $K = 0.25$ and $r_{eq} = 0.85$. The other is the *non-crossing spring*, which is defined by the parameters $K = 1.0$ and $r_{eq} = 0.65$. From the results of the last section, the *crossing springs* pass freely through each other, while the *non-crossing springs* pass through each other much less frequently. Note that the *non-crossing springs* have a shorter radius of gyration due to the shorter bead separation and so the radius of the particle is adjusted to keep the relative polymer lengths and relative polymer surface densities equal. The results are shown in Table VII.

With the *non-crossing springs*, where polymer crossing is greatly reduced, it takes a much longer time for the colloidal particles to adsorb than with the *crossing springs*. The polymers with the *non-crossing springs* are much more difficult for a particle to penetrate because the polymers become entangled together, thus greatly restricting their movement. This means that the polymers find it much more difficult to move out the way of an approaching colloidal particle, as illustrated by Figure 18.

5.4. Summary

A polymer crossing model, consisting of two interlocked polymer rings, has been constructed for studying the extent of polymer crossing in dense

TABLE VII The effect of the extent of polymer crossing on the adsorption of a colloidal particle onto a polymer coated surface

Polymer surface density	*Spring type*	*Radius of gyration*	*Radius of particle*	*Adsorption time (time unit)*
0.7	crossing	1.49	1.49	220,200
0.7	non-crossing	1.29	1.29	> 300,000

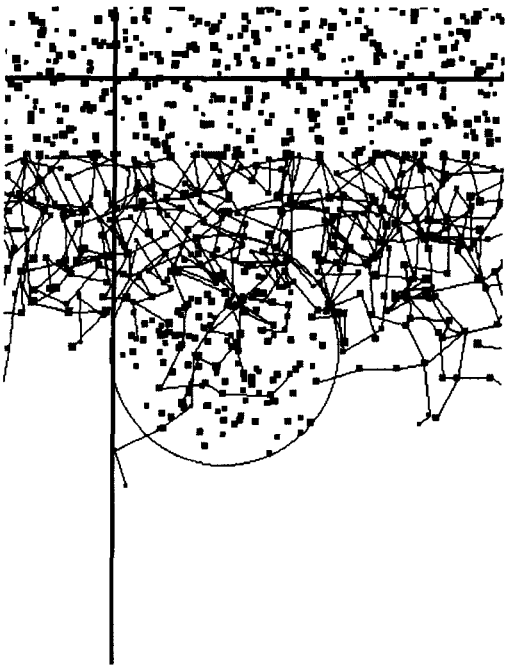

FIGURE 18 An entangled polymer layer blocking the approach of a colloidal particle.

systems. Two major factors, spring constant and spring length, have been identified as having a significant effect on polymer crossing. By adjusting these two parameters, one can reduce the extent of polymer crossing and obtain what we have called *non-crossing springs*, therefore achieving more realistic simulations. In the case of the adsorption of colloidal particles onto a polymer coated surface, the simulation results showed that with the *non-crossing springs*, where polymer crossing is greatly reduced, it is much more difficult for the colloidal particles to penetrate the polymer layer and adsorb onto the surface than with the *crossing springs*. This is due to the polymers with the *non-crossing springs* becoming entangled together, thus greatly restricting their movement.

6. AN INVESTIGATION INTO THE VISCOSITY OF COLLOID-POLYMER SYSTEMS

As mentioned in the introduction, the motivation behind this work was the problem of controlling the effects of soot in diesel engine lubricating oil. The

oil becomes contaminated by soot particles of 10 to 50 nm in size, created by incomplete fuel combustion, which alter the rheology of the lubricating oil [19]. The soot particles experience the conditions of time and temperature necessary to agglomerate, which adversely affects the viscosity of the oil. As the concentration of soot in the oil increases, the viscosity of the oil increases. When the concentration of soot is sufficiently high the oil forms a gel, changing to a *thixotropic* fluid, a fluid in which the shear stress decreases with time as the fluid is sheared. Dispersants are added to the oil in an attempt to control the extent of the agglomeration [2]. However, the presence of these dispersants will also affect the shear viscosity of the oil, especially when interacting with the soot particles. Therefore, in this section a study is presented on the effect of the presence of soot agglomerates and dispersants on the viscosity of the oil in the early stages of this process. An understanding of this relationship should help in optimising the properties of the dispersant.

6.1. The Viscosities of Different Systems

The viscosities of the following five systems have been studied:

1. *Pure solvent.* The system consists of solvent particles only.
2. *Solution of soot.* The system consists of solvent and soot particles only. Eleven soot particles of radius 1.2, making a volume fraction of 8%. The density of a soot particle is 2.35 times that of the solvent.
3. *Solution of polymers.* The system consists of solvent and polymers only. There are 110, 5-bead, *non-crossing* polymers in the system, consisting of approximately the same number of DPD particles as were contained in the soot particles of system 2.
4. *Solution of soot with free polymers.* The system consists of solvent, soot particles and free polymers (free meaning that the polymers are not attached to a soot particle or surface). The interaction between the different parts of the system is neutral so that the soot particles will not agglomerate and the polymers will stay free. The solution contains the same number and size of soot particles as system 2 and the same number and size of polymers as system 3.
5. *Solution of soot with attached polymers.* This is the same as system 4 but with the polymers no longer free. Instead they are evenly distributed among the soot particles, with one end of each polymer randomly attached onto the surface of its associated soot particle, so that the polymer surface density is about 0.55.

All the simulations were conducted in a neutral solvency environment (*i.e.*, $\xi = 0$), with a simulation box of size $10 \times 10 \times 10$ and $\delta t = 0.25$. The solvent density was always 3. Each system was initially simulated at shear rates of both 0.005 and 0.002 to ensure that the viscosity being measured was in the first Newtonian regime for the fluid (*i.e.*, the region of constant viscosity before shear-thinning occurs). If these two shear rates gave the same viscosity, then the result was accepted, otherwise, as with system 5, the shear rate was lowered further until consistent results were obtained. The results are listed in Table VIII, where the reduced viscosity is calculated as the suspension viscosity divided by that of the pure solvent. The value quoted for system 5 is at a shear rate of 0.001 (refer to Fig. 20 to see how its value varies). The results show that addition of soot alone (solution of soot) has a slightly weaker affect on the viscosity than when just polymers are added (solution of polymers). In the combination of these two systems (soot with free polymers), the change in viscosity is approximately the addition of that of the two individual systems. When the polymers are attached to the soot particles, the viscosity is significantly increased.

The remainder of this viscosity study focuses on systems 2 and 5 only.

6.2. The Variation of Viscosity with Soot Volume Fraction

Several different volume fractions of soot were simulated and the viscosity of the solution determined for each. The other parameters were the same as system 2 of §6.1. The reduced viscosity is shown as the solid line in Figure 19. The Einstein result ($1 + 2.5c$ where c is the volume fraction) is also displayed. The curve of our results shows a good fit to the Einstein result at low volume fractions. This is in agreement with the results of Koelman and Hoogerbrugge [5] and a useful validation of our model.

6.3. The Variation of Viscosity with Shear Rate

System 5 defined in §6.1 was used in the study. The shear-thinning curve of reduced viscosity against shear rate is shown in Figure 20. A strong shear thinning is observed as shear rate increases.

TABLE VIII The viscosities of the different systems

System	*Reduced viscosity*
1. Pure solvent	1.00
2. Solution of soot	1.23
3. Solution of polymers	1.25
4. Soot with free polymers	1.52
5. Soot with attached polymers	2.31

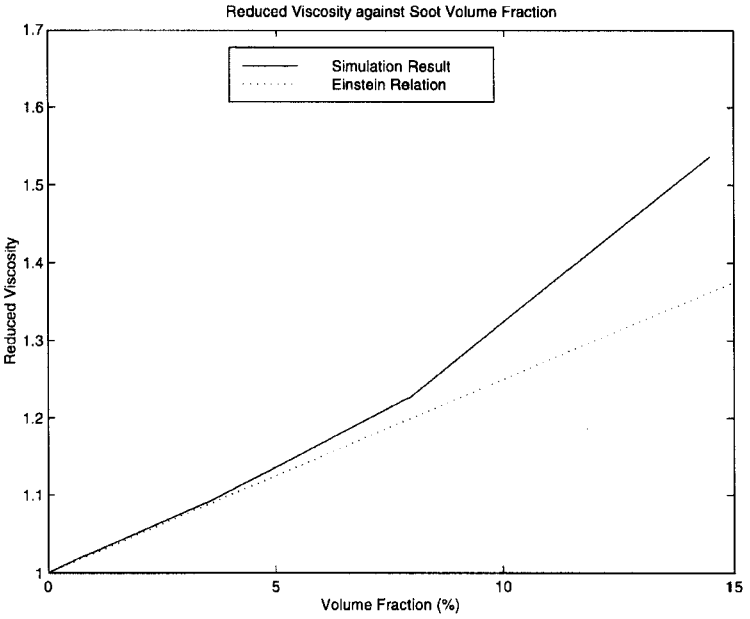

FIGURE 19 The variation of reduced viscosity with soot volume fraction.

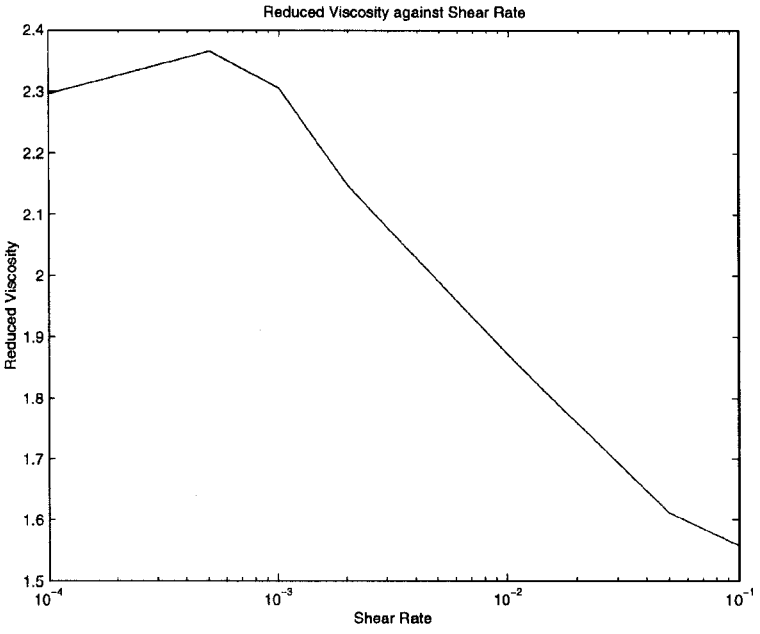

FIGURE 20 The variation of reduced viscosity with shear rate.

6.4. The Variation of Viscosity with the Polymer Surface Density on the Soot Particles

Again, system 5 defined in §6.1 was used as the basis for this study. All the simulations were conducted at a shear rate of 0.001. The polymer surface density on the soot particles was varied to determine its influence on the viscosity. Two different soot volume fractions were investigated. The results (see Fig. 21) show that the higher the polymer surface density of the soot, the higher the viscosity. The two lines are close to parallel up to a surface density of about 0.8, where the lower volume fraction starts to increase its viscosity more quickly and crosses over the other line.

6.5. The Variation of Viscosity with Polymer Solvency

Given that the systems used in this study are far more complex than the dilute polymer solutions used in previous studies [6–8], it is anticipated that the behaviour of our soot-polymer systems will also be more complex. Once more, system 5 defined in §6.1 was used as the basis for this study, with a

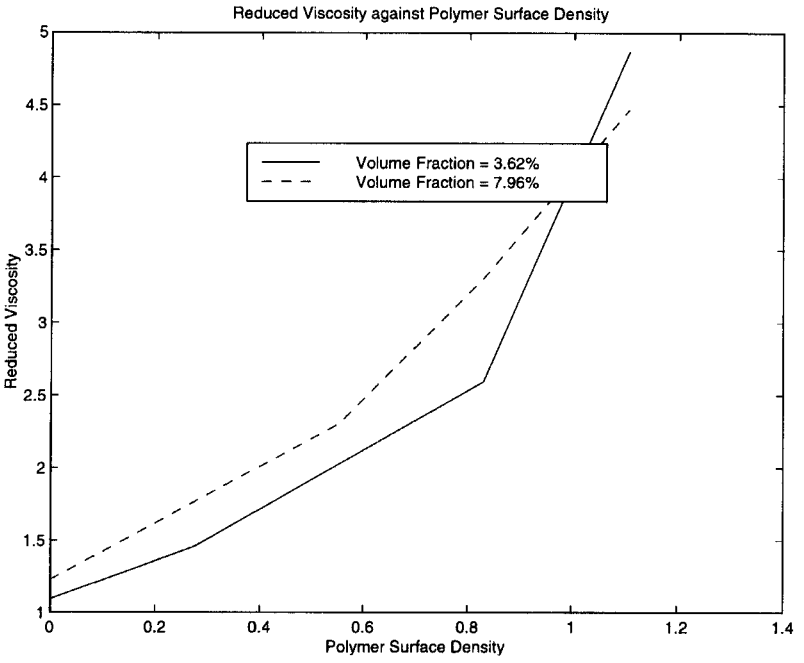

FIGURE 21 The variation of reduced viscosity with the polymer surface density on the soot particles.

shear rate of 0.001 throughout. Three different polymer-soot systems were configured for comparison. They are five-bead polymers with a density of 0.55, five-bead polymers with a density of 0.83 and six-bead polymers with a density of 0.55. Only the polymer solvency is being studied; the soot solvency will remain neutral.

The curves of reduced viscosity against solvent quality are shown in Figure 22. The reduced viscosity was measured for good ($\xi = -0.3$), neutral ($\xi = 0.0$) and poor ($\xi = 0.3$) solvency cases. The straight lines drawn on the graph are merely to guide the eye. The viscosity is only slightly affected as the solvency changes from good to neutral. From neutral to poor solvency, there is a much bigger difference. The three curves converge to about the same value since when the polymers have collapsed, the density and length makes very little difference. Generally speaking, when the solvency is neutral or better, the polymer coated soot particles will stay apart, as shown in Figure 23. Conversely, when the solvency is poor, the polymer coated soot particles will collapse or aggregate, as shown in Figure 24. When the configuration changes from the dispersed phase of Figure 23 to the collapsed phase of

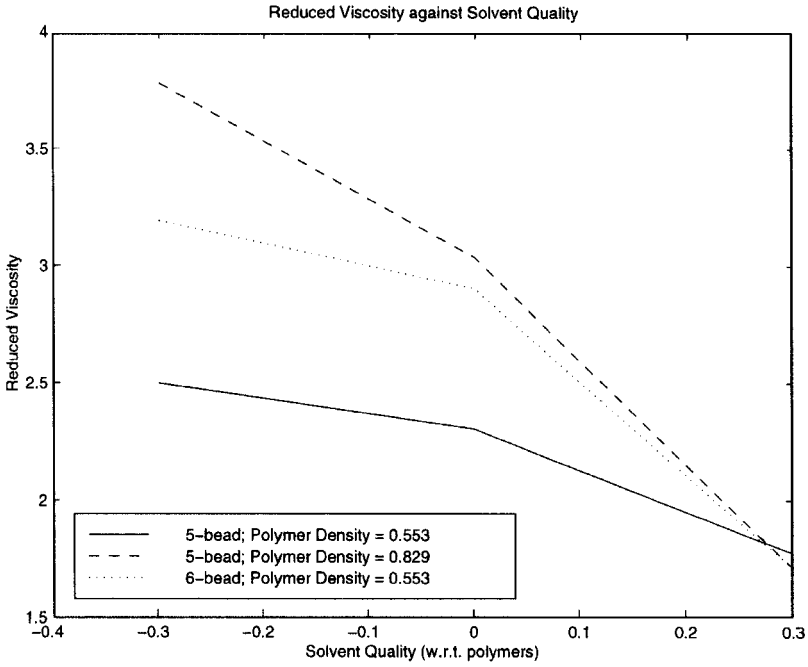

FIGURE 22 The variation of viscosity with polymer solvency.

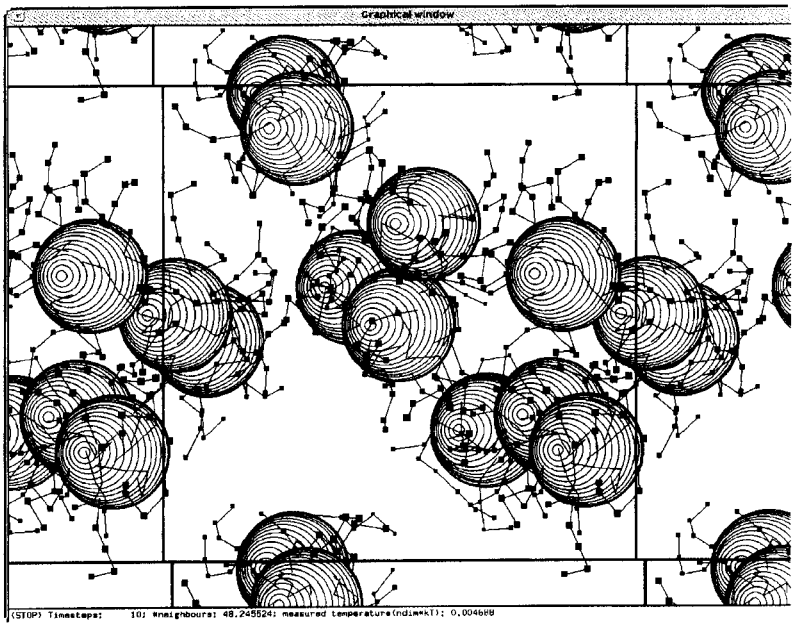

FIGURE 23 The configuration of the polymer coated soot particles in a neutral or good solvent.

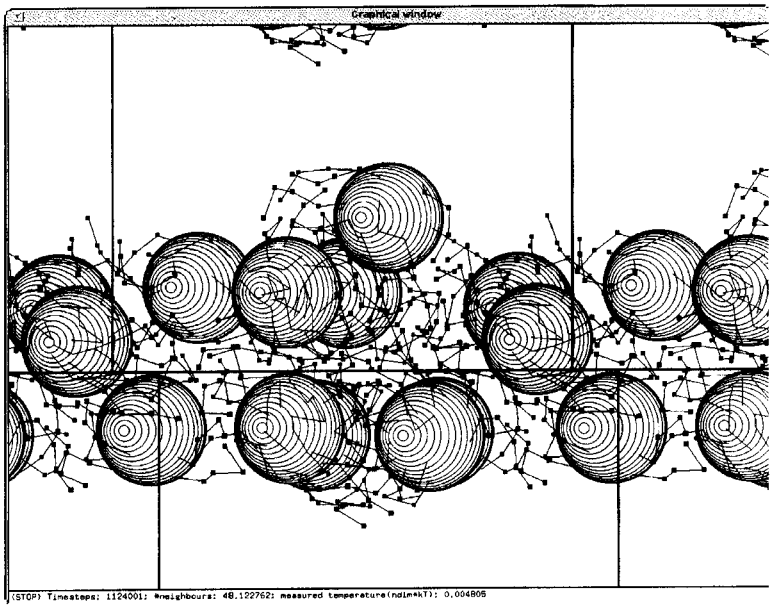

FIGURE 24 The configuration of the polymer coated soot particles in a poor solvent.

Figure 24, the viscosity of the system decreases due to the reduction in the interface fraction between the solvent and the polymer coated soot particles.

6.6. Summary

The study showed that addition of soot alone (solution of soot) has a slightly weaker affect on the viscosity then when just polymers are added (solution of polymers). However, when the polymers are attached to the soot particles, the viscosity is significantly higher than either of the two stand-alone cases. The variation of reduced viscosity with soot volume fraction showed good agreement with the Einstein result. The shear-thinning curve was obtained for the polymer coated soot solution. The polymer density on the soot particles was varied and showed that viscosity increases with polymer density. Finally, the effect of polymer solvency on viscosity was studied for the polymer coated soot solution. We found that different solvent qualities can result in different soot-polymer configurations, which lead to changes in viscosity. Generally speaking, when the solvency is neutral or better, the polymer coated soot particles will stay part. Conversely, when the solvency is poor, the polymer coated soot particles will collapse or aggregate. When the configuration changes from the dispersed phase to the collapsed phase, the viscosity of the system decreases due to the reduction in the interface fraction between the solvent and the polymer coated soot particles.

7. CONCLUSIONS

The results are consistent with what might be expected from physical reasoning. A greater understanding of the model used has also allowed refinements to be made to previous versions, such as the introduction of virtual walls or in the control of polymer crossing. We have shown that the DPD model presented here is potentially a very useful tool in the understanding of the behaviour of a solvent-colloid-polymer system.

Acknowledgements

The authors are grateful to Prof. R. C. Coy, Dr. W. D. Cooper, Dr. A. D. H. Clague and Dr. R. I. Taylor for their enthusiastic advice and to Shell Research Ltd. for its financial support and permission to publish. J. B. Gibson would also like to acknowledge financial support from an EPSRC CASE studentship with Shell Research Ltd.

References

[1] Gibson, J. B., Chen, K. and Chynoweth, S. (1998). "Simulation of Particle Adsorption onto a Polymer Coated Surface using the Dissipative Particle Dynamics Method", *J. Colloid Interface Sci.*, **206**, 464.

[2] Bezot, P., Hesse-Bezot, C. and Diraison, C. (1997). "Aggregation Kinetics of Colloidal Suspensions of Engine Soots. Influence of Polymeric Lubricant Additives", *Carbon*, **35**, 53.

[3] Hoogerbrugge, P. J. and Koelman, J. M. V. A. (1992). "Simulating Microscopic Hydrodynamic Phenomena with Dissipative Particle Dynamics", *Europhys. Lett.*, **19**, 155.

[4] Español, P. and Warren, P. (1995). "Statistical-Mechanics of Dissipative Particle Dynamics", *Europhys. Lett.*, **30**, 191.

[5] Koelman, J. M. V. A. and Hoogerbrugge, P. J. (1993). "Dynamic Simulations of Hard-Sphere Suspensions under Steady Shear", *Europhys. Lett.*, **21**, 363.

[6] Kong, Y., Manke, C. W., Madden, W. G. and Schlijper, A. G. (1994). "Simulation of a Confined Polymer in Solution using the Dissipative Particle Dynamics Method", *Int. J. Thermophys.*, **15**, 1093.

[7] Schlijper, A. G., Hoogerbrugge, P. J. and Manke, C. W. (1995). "Computer Simulation of Dilute Polymer Solutions with the Dissipative Particle Dynamics Method", *J. Rheol.*, **39**, 567.

[8] Kong, Y., Manke, C. W., Madden, W. G. and Schlijper, A. G. (1997). "Effect of Solvent Quality on the Conformation and Relaxation of Polymers via Dissipative Particle Dynamics", *J. Chem. Phys.*, **107**, 592.

[9] Coveney, P. V. and Novik, K. E. (1996). "Computer Simulations of Domain Growth and Phase Separation in Two-Dimensional Binary Immiscible Fluids Using Dissipative Particle Dynamics", *Phys. Rev. E.*, **54**, 5134.

[10] Coveney, P. V. and Novik, K. E. (1997). "Using Dissipative Particle Dynamics to Model Binary Immiscible Fluids", *Int. J. Mod. Phys. C.*

[11] Boek, E. S., Coveney, P. V. and Lekkerkerker, H. N. W. (1996). "Computer Simulation of Rheological Phenomena in Dense Colloidal Suspensions with Dissipative Particle Dynamics", *J. Phys. Condens. Mat.*, **8**, 9509.

[12] Boek, E. S., Coveney, P. V., Lekkerkerker, H. N. W. and van der Schoot, P. (1997). "Simulating the Rheology of Dense Colloidal Suspensions using Dissipative Particle Dynamics", *Phys. Rev. E.*, **55**, 3124.

[13] Español, P. (1995). "Hydrodynamics from Dissipative Particle Dynamics", *Phys. Rev. E*, **52**, 1734.

[14] Español, P. (1997). "Dissipative particle dynamics with energy conservation", *Europhys. Lett.*, **40**, 631.

[15] Avalos, J. B. and Mackie, A. D. (1997). "Dissipative particle dynamics with energy conservation", *Europhys. Lett.*, **40**, 141.

[16] Groot, R. D. and Warren, P. B. (1997). "Dissipative Particle Dynamics: Bridging the gap between Atomistic and Mesoscopic Simulation", *J. Chem. Phys.*, **107**, 4423.

[17] Forrest, B. M. and Suter, U. W. (1995). "Accelerated equilibration of polymer melts by time coarse-graining", *J. Chem. Phys.*, **102**, 7256.

[18] Marsh, C. A. and Yeomans, J. M. (1997). "Dissipative Particle Dynamics: The Equilibrium for Finite Time Steps", *Europhys. Lett.*, **37**, 511.

[19] Seifert, W. W. and Desjardins, J. B. (1995). "Measurement of Soot in Diesel Engine Lubricating Oil", SAE Technical Paper Series, 951023.